Journal of Advanced Research 16 (2019) 113–122

Contents lists available at ScienceDirect

Journal of Advanced Research

journal homepage: www.elsevier.com/locate/jare

Original Article

Probing the complex thermo-mechanical properties of a 3D-printed polylactide-hydroxyapatite composite using *in situ* synchrotron X-ray scattering

Tan Sui [a,b,*], Enrico Salvati [a], Hongjia Zhang [a], Kirill Nyaza [c,d], Fedor S. Senatov [d], Alexei I. Salimon [c,d], Alexander M. Korsunsky [a,c,*]

[a] Department of Engineering Science, University of Oxford, Parks Road, Oxford OX1 3PJ, United Kingdom
[b] Department of Mechanical Engineering Sciences, University of Surrey, Guildford, Surrey GU2 7XH, United Kingdom
[c] Skoltech - Skolkovo University of Science and Technology, Nobel St., 3, Moscow 143026, Russian Federation
[d] National University of Science and Technology "MISIS", 119049, Leninsky Prospect, 4, Moscow, Russian Federation

HIGHLIGHTS

- *In situ* synchrotron X-ray study of PLA-HAp composite multi-scale thermo-mechanics.
- Mullins effect attributed to non-linear strain interaction of PLA lamella with HAp.
- Reversible PLA phase transformation at ~60 °C, and irreversible above 92 °C.
- Compression → tension change of PLA lamella strain under tensile load & temperature.
- Addition of HAp filler enhances PLA shape memory effect and mechanical properties.

GRAPHICAL ABSTRACT

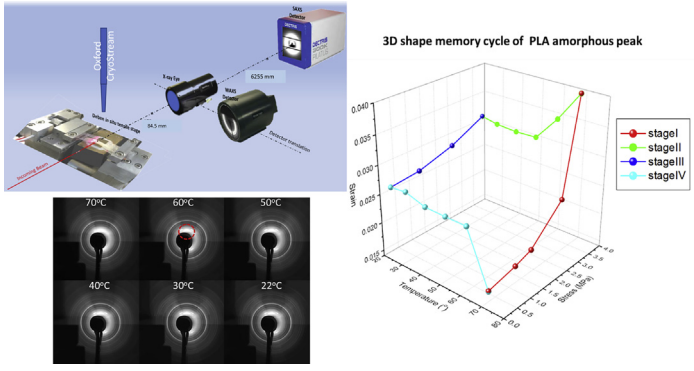

ARTICLE INFO

Article history:
Received 31 August 2018
Revised 7 November 2018
Accepted 7 November 2018
Available online 16 November 2018

Keywords:
3D-printed polylactide-hydroxyapatite composite
Mullins effect
Thermo-mechanical behaviour
Shape memory effect
Small- and wide-angle X-ray scattering

ABSTRACT

Polylactide (PLA)-hydroxyapatite (HAp) composite components have attracted extensive attentions for a variety of biomedical applications. This study seeks to explore how the biocompatible PLA matrix and the bioactive HAp fillers respond to thermo-mechanical environment of a PLA-HAp composite manufactured by 3D printing using Fused Filament Fabrication (FFF). The insight is obtained by *in situ* synchrotron small- and wide- angle X-ray scattering (SAXS/WAXS) techniques. The thermo-mechanical cyclic loading tests (0–20 MPa, 22–56 °C) revealed strain softening (Mullins effect) of PLA-HAp composite at both room and elevated temperatures (<56 °C), which can be attributed primarily to the non-linear deformation of PLA nanometre-scale lamellar structure. In contrast, the strain softening of the PLA amorphous matrix appeared only at elevated temperatures (>50 °C) due to the increased chain mobility. Above this temperature the deformation behaviour of the soft PLA lamella changes drastically. The thermal test (0–110 °C) identified multiple crystallisation mechanisms of the PLA amorphous matrix, including reversible stress-induced large crystal formation at room temperature, reversible coupled stress-temperature-induced PLA crystal formation appearing at around 60 °C, as well as irreversible heating-induced crystallisation above 92 °C. The shape memory test (0–3.75 MPa, 0–70 °C) of the PLA-HAp composite demonstrates a fixing ratio (strain upon unloading/strain before unloading) of 65% and rather a ~100% recovery ratio, showing

Peer review under responsibility of Cairo University.
* Corresponding authors.
E-mail addresses: t.sui@surrey.ac.uk (T. Sui), alexander.korsunsky@eng.ox.ac.uk (A.M. Korsunsky).

https://doi.org/10.1016/j.jare.2018.11.002
2090-1232/

an improved shape memory property. These findings provide a new framework for systematic characterisation of the thermo-mechanical response of composites, and open up ways towards improved material design and enhanced functionality for biomedical applications.

Introduction

3D printing (3DP) technology has great potential in biomedical engineering applications, leading to fast development of materials systems available for 3DP [1]. Many poly(α-hydroxy esters), such as polylactide (PLA), have been shown to have high biocompatibility, degradability and low immunogenicity, and therefore have been widely used in biomedical applications such as stents, soft-tissue implants, and tissue engineering scaffolds [2–6]. In these applications PLA is exposed to different device-specific loading environments. The rate of degradation of PLA is dependent on the magnitude of the applied stress [7,8], and its mechanical response is highly non-linear due to a strong dependence on temperature. Therefore, it is critically important to understand the thermo-mechanical properties of PLA to optimise device design to avoid unexpected rupture and failure. In addition, the thermo-mechanical properties of PLA can be modified by many different methods, including thermal heat treatments and adding fillers [9,10]. Bioactive ceramic fillers, such as hydroxyapatite (HAp), are most commonly used to enhance the mechanical properties of the polymer matrix, and to improve the bioactivity and osteoconductivity of the polymer composite, including PLA-based composite [11]. The PLA-HAp composite has recently attracted extensive attention for a variety of biomedical applications [12,13].

Among various experimental techniques on investigating thermo-mechanical properties of polymer materials at the macroscopic level, synchrotron X-ray techniques are nowadays well established for *in situ* evaluation of structural evolution across the length scales of many types of elastomers, e.g. natural rubber, polyurethane, as well as PLA [14–17], and allows revealing the intricate relationships between the structure and thermo-mechanical loading non-destructively. Small- angle X-ray scattering (SAXS) is widely used to obtain quantitative structural information and evolution in both crystalline and amorphous materials at the nano-scale, whereas wide- angle X-ray scattering (WAXS) is broadly applied to quantify the crystallographic properties and crystal lattice strain at the angstrom-scale in response to the external load [18,19]. However, most effort of using synchrotron X-ray techniques so far has been devoted to the characterisation of single phase PLA materials [14,15], with little attention devoted to the exploration of PLA-based composites. The deep insight of the polymer matrix phase transformation induced by temperature or stress and its interaction with additional reinforcement phases (e.g. bio-fillers) are needed. Only the non-destructive, multi-scale and *in situ* capability that synchrotron-based SAXS/WAXS methods have would address these questions of how additional reinforcement phases interact and affect the polymer matrix in terms of strain softening mechanism, crystallisation mechanisms, as well as the shape memory effect.

The motivation of this study was to address the need for better understanding of the interaction between the PLA matrix and HAp fillers, in a PLA-based composite that is manufactured by fused filament fabrication (FFF). In particular, attention was devoted to the impact of the phases on the Mullins effect, thermal properties, thermo-mechanical behaviour, and shape memory effect. *In situ* SAXS/WAXS was employed to probe the structural evolution of the PLA amorphous matrix, PLA lamella structure and HAp crystals under various thermo-mechanical regimes. The critical insights obtained provide firm observational basis for improved design and enhanced functionalities.

Material and methods

Sample preparation

Polylactide (PLA) with molecular weight 110 kg/mol (Ingeo 4032D, Natureworks LLC, MN 55345, USA) and 15 wt% hydroxyapatite (HAp) powder (nominal size 90 ± 10 nm, JSC Polystom, Moscow, Russia) were mixed by a screw extruder HAAKE MiniLab II Micro Compounder (Thermo Fisher Scientific, Waltham, USA). Screw speed and dwell time were optimised to ensure the uniform mixing and reduce the defects formed during the extrusion. Filaments of PLA-HAp composite were obtained with the diameter of ~1.6 mm for the 3D printing. CubePro Trio (3D Systems, Rock Hill, USA) was used to produce a sheet of 3D printed PLA-based composite with a nozzle diameter of 350 μm at 210 °C. Detailed preparation route was described in a previous publication [20]. Samples were cut from the sheet with a thickness of 500 μm. The cross-sectional dimensions of samples and grip-to-grip length were measured before the mechanical or thermo-mechanical tests for converting the load and displacement into stress and strain.

In situ synchrotron X-ray scattering experiment

The experiment was performed on B16 beamline at Diamond Light Source (DLS, Harwell, UK). 18 keV monochromatic beam was used with a beam spot size of 150 μm×150 μm. MicroTest tensile loading rig (Deben Ltd, Bury St Edmunds, UK) with a 200 N calibrated load cell was used for thermo-mechanical testing. Cryostream Plus (OxfordCryosystems, Long Hanborough, Oxford, UK) was applied to create the target temperature environment for each sample. The combination of Deben and Cryostream Plus allows the coupled thermo-mechanical and shape memory effect characterisations. "X-ray Eye" imaging detector (sCMOS camera, Photonic Science Ltd., Mountfield, UK) was initially used to identify the region of interest (ROI) on each sample. WAXS detector (Image Star 9000, Photonic Science Ltd., Mountfield, UK) was positioned at the sample-to-detector distance of 84.5 mm for WAXS pattern acquisition and the distance was calibrated by the standard silicon powder (NIST SRM 640d) and Lanthanum hexaboride (LaB6, NIST SRM 660a). Pilatus 300 K SAXS detector (Dectris, Baden, Switzerland) was positioned at the sample-to-detector distance of 6255 mm for SAXS pattern acquisition and the distance was calibrated by the non-crystalline standard dry chicken collagen [21].

Using the set-up described above and illustrated in Fig. 1a, the following experiments were performed.

(i) Mullins effect: sample was clamped and deformed by the Deben MicroTest loading rig. Seven incremental loading-unloading cycles of uniaxial tensile test were conducted at room temperature with the maximum load achieved at each cycle being 5 MPa, 10 MPa, 15 MPa, 20 MPa, 25 MPa, 30 MPa and 35 MPa. For each cycle, nine loading and unloading increments were defined and a WAXS pattern was acquired at each increment.

(ii) Thermal properties: sample was placed under the Cryostream Plus nozzle and heated up from room temperature (22 °C) to 110 °C, followed by cooling down to room temperature again with a constant rate of 2 °C/min. The WAXS pattern was collected at each degree centigrade.

(iii) Thermo-mechanical behaviour: Cryostream Plus was set for the following temperatures: 22 °C, 50 °C, 52 °C, 54 °C and 56 °C. At each temperature, the sample was subjected to the maximum applied load of 20 MPa with nine loading and unloading increments, followed by heating up to the next temperature. The sample finally failed at 56 °C upon loading to 20 MPa. The WAXS patterns were obtained at each loading/unloading increment.

(iv) Shape memory effect: the initial stage and four additional stages were used to construct the overall 3D shape memory cycle characterisation. At the initial stage the sample was heated up from 22 °C to 70 °C under the small load of 0.25 MPa. Afterwards, at stage I, the temperature was kept at 70 °C and a load was increased from 0.25 MPa to 3.75 MPa in 5 increments. At stage II, the load was kept at 3.75 MPa, and the temperature reduced from 70 °C to room temperature with an increment of −10 °C. At stage III, the sample was unloaded from 3.75 MPa to 0.25 MPa in 4 increments. At the final stage IV, the load of 0.25 MPa was kept constant, and the sample was heated up to 70 °C with an increment of 10 °C. At each temperature/load increment, the WAXS pattern was captured.

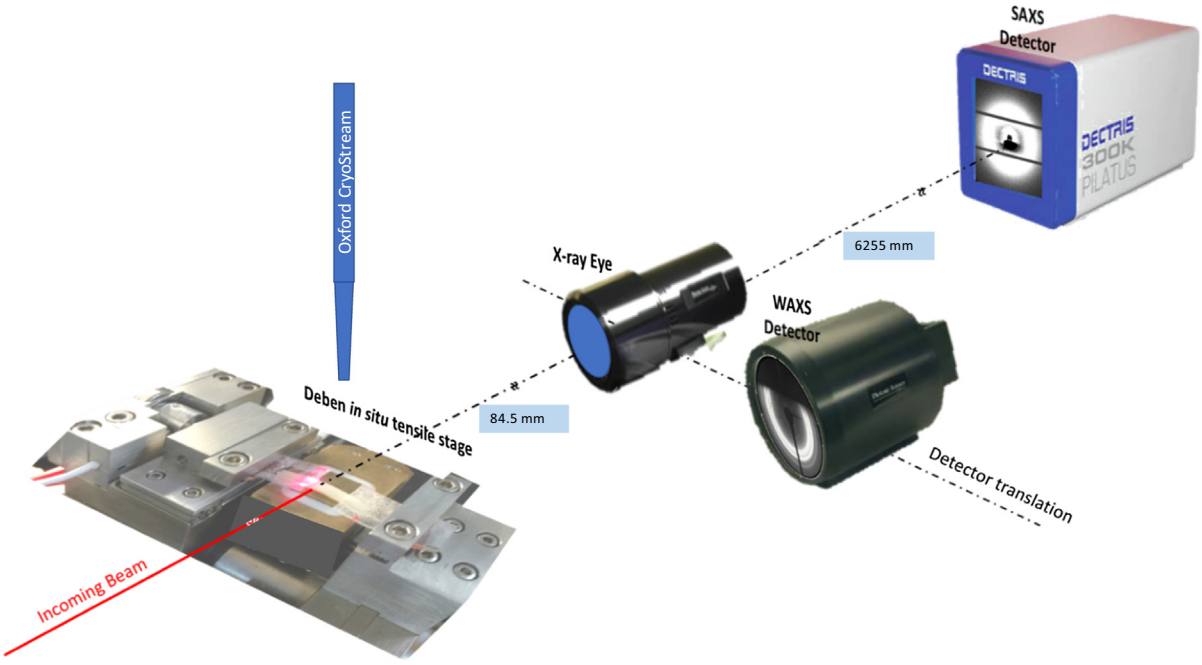

(a)

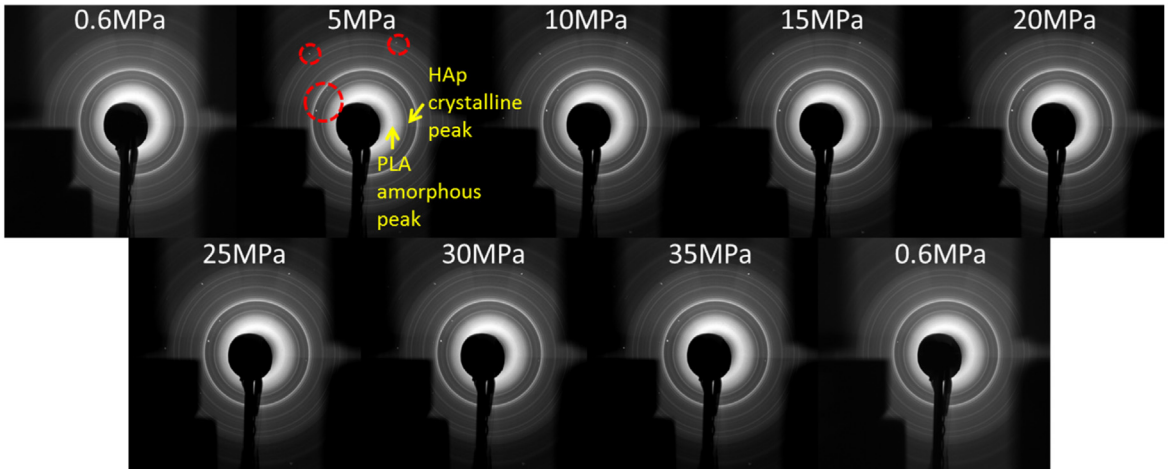

(b)

Fig. 1. Experimental setup, 2D SAXS/WAXS patterns, and 1D profiles for data interpretation. (a) Experimental setup incorporating the thermo-mechanical loading rig, imaging detector ("X-ray eye"), WAXS and SAXS detectors. (b) 2D WAXS patterns at initial state, maximum load at each cycle and final state. Examples of isolated bright diffraction spots are highlighted in red dash circles; (c) 2D SAXS patterns at initial state, maximum load at each cycle and final state; (d) 1D line profiles of WAXS patterns at corresponding states in (a); and (e) 1D electron density correlation functions from SAXS patterns for lamella structure analysis.

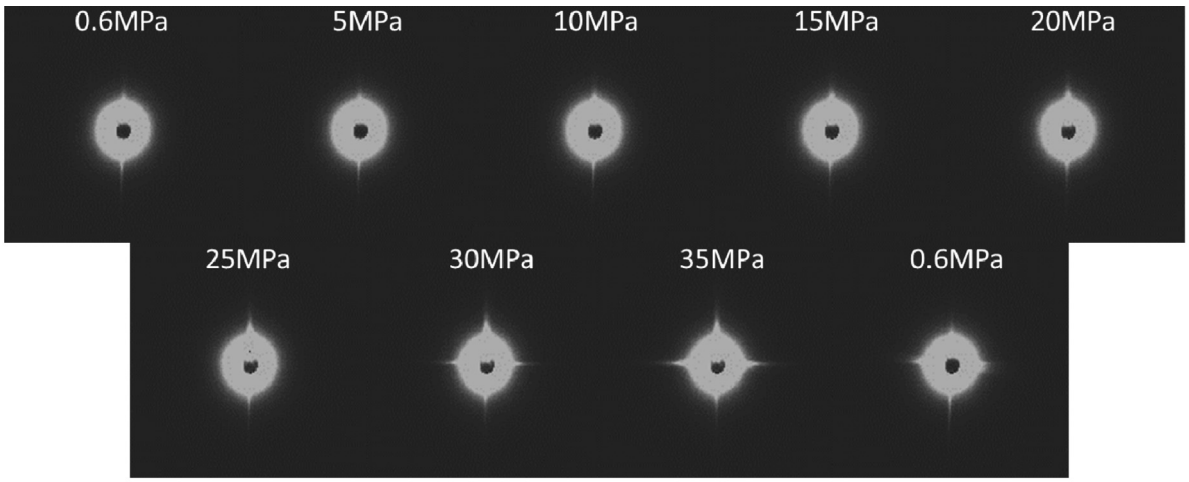

(c)

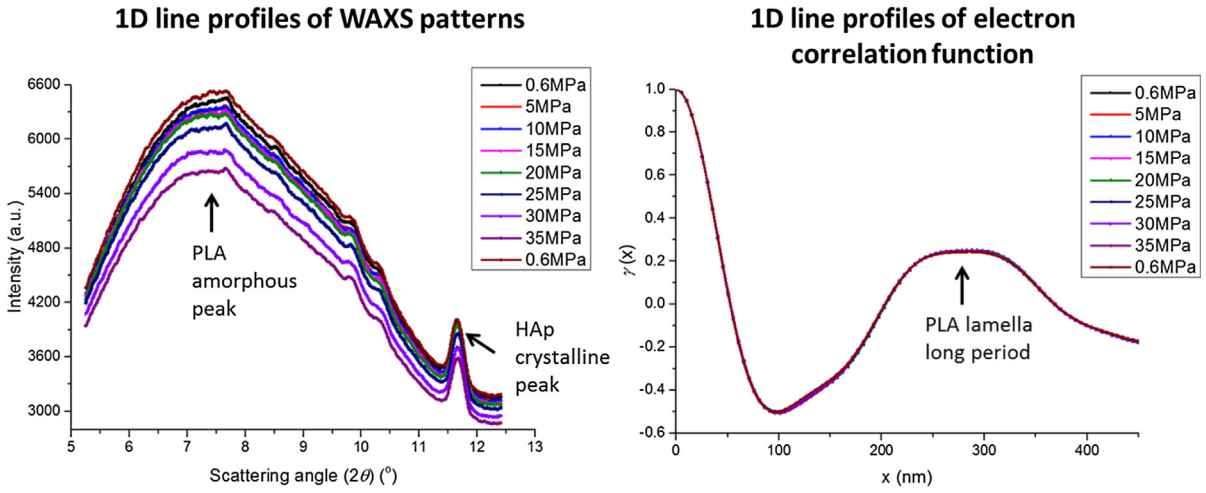

(d) (e)

Fig. 1 (*continued*)

Data interpretation

The macroscopic deformation data was exported from Microtest software (Deben, Bury St Edmunds, UK). Temperature information was saved in the data file that corresponds to each diffraction file. 2D WAXS patterns (e.g. Fig. 1b) were converted into 1D line profiles $I(2\theta)$ as a function of the scattering angle 2θ by integrating over a range of azimuthal angles (±20°) for the quantitative analysis. The peaks corresponding to the "PLA amorphous peak" and "HAp crystalline peak" were illustrated in Fig. 1d. The peaks were fitted as Gaussian peaks to determine their center positions. The strains for PLA matrix and HAp fillers peaks were calculated from the shift of the peak center positions with respect to the initial strain-free reference condition respectively. The detailed analysis procedure of WAXS data interpretation has been described in our previous work [19,22]. 2D SAXS patterns (e.g. Fig. 1c) were processed into 1D intensity profiles $I(q)$ as a function of the scattering vector q. Then 1D electron density correlation function was calculated according to the following function $\gamma(x) = \int_0^\infty I(q)q^2 \cos(qx)dq / \int_0^\infty I(q)q^2 dq$ [23]. The peaks corresponding to the "PLA lamella long period" structure were illustrated in Fig. 1e. The centre position of each peak was determined by Gaussian fitting function. The PLA lamella structure strain evolution was then deduced for each "PLA lamella long period" peak from the shift of the peak center position.

Results

Mullins effect

Snapshots of 2D WAXS and SAXS patterns of the PLA-HAp composite are shown in Fig. 1b and c, consisting of the patterns at the initial state (0.6 MPa), at the maximum load for each cycle (5 MPa, 10 MPa, 15 MPa, 20 MPa, 25 MPa, 30 MPa and 35 MPa), and the final unloaded state (0.6 MPa) after seven cycles. Isolated bright diffraction spots appear in WAXS patterns (indicated by red dashed circles in Fig. 1b) at high load, indicating the strain-induced formation of "large" crystals. This crystallization phenomenon is reversible as diffraction spots disappear when the load is released. Changes are also observed in SAXS patterns as the scattering streaks appear in the meridional direction for the first five cycles, and also appear equatorially at higher loads, which indicates the re-alignment of chain structures. Fig. 1d shows the corresponding 1D radial line profiles of the WAXS patterns and highlights the amorphous peaks from PLA and crystalline peaks from HAp filler

used for quantitative strain analysis. The corresponding 2D patterns are marked in Fig. 1b. Fig. 1e displays the 1D electron density functions derived from SAXS patterns for quantifying the strain evolution in the PLA lamella structure.

The macroscopic strain evolution of PLA-HAp composite measured by Deben is plotted in Fig. 2a, showing typical non-linear stress-strain curves of elastomers at the macroscopic level. The softening phenomenon is visible in Fig. 2a, as the slope of the unloading curve decreases over seven cycles. PLA strain evolution obtained by interpreting the amorphous peak of WAXS patterns is shown in Fig. 2b. The deformation is found to be close to linear in each cycle without any obvious softening, as the loading-unloading path remains almost the same over all the cycles. In contrast, HAp fillers exhibit highly non-linear deformation behaviour as shown in Fig. 2c with a varying slope, following the similar behaviour at macroscopic level (Fig. 2a). Note that HAp fillers undergo compression in all tested cycles, and that the strain magnitude is approximately one tenth of the PLA amorphous matrix deformation (Fig. 2b), and one hundredth that of macroscopic deformation (Fig. 2a). Trend of the deformation of the PLA lamella structure resembles that of the HAp fillers as shown in Fig. 2d, which also displays compressive deformation with significant non-linear behaviour.

Thermal properties

The PLA amorphous peaks are chosen to visualise the thermal properties and the results are shown in Fig. 3. The scattering angles are observed to decrease from room temperature to about 92 °C in two linear stages (marked in red in Fig. 3) with two different slopes (steeper in the second stage), with the slope change occurring at about 60 °C representing the first phase transition. In each stage, the PLA amorphous matrix expands linearly as the temperature increases (as the scattering angles are inversely related to the structure size in the real space). Beyond 92 °C, the scattering angles demonstrate a dramatic increase up to 99 °C and subsequently gradually stabilize until the final temperature at 110 °C. This indicates the second phase transition that happens around 90–100 °C. Afterwards, during the cooling process of the PLA-HAp composite down to the room temperature, the scattering angles further increase linearly with a moderate slope. In Fig. 3, several selected 2D WAXS patterns are displayed around the phase transition temperatures. Comparing the patterns at 60 °C and 92 °C, no obvious change can be seen for the first phase transition at 60 °C. However, an additional diffraction ring appears in the pattern at 110 °C compared with that at 92 °C, demonstrating the occurrence of rapid

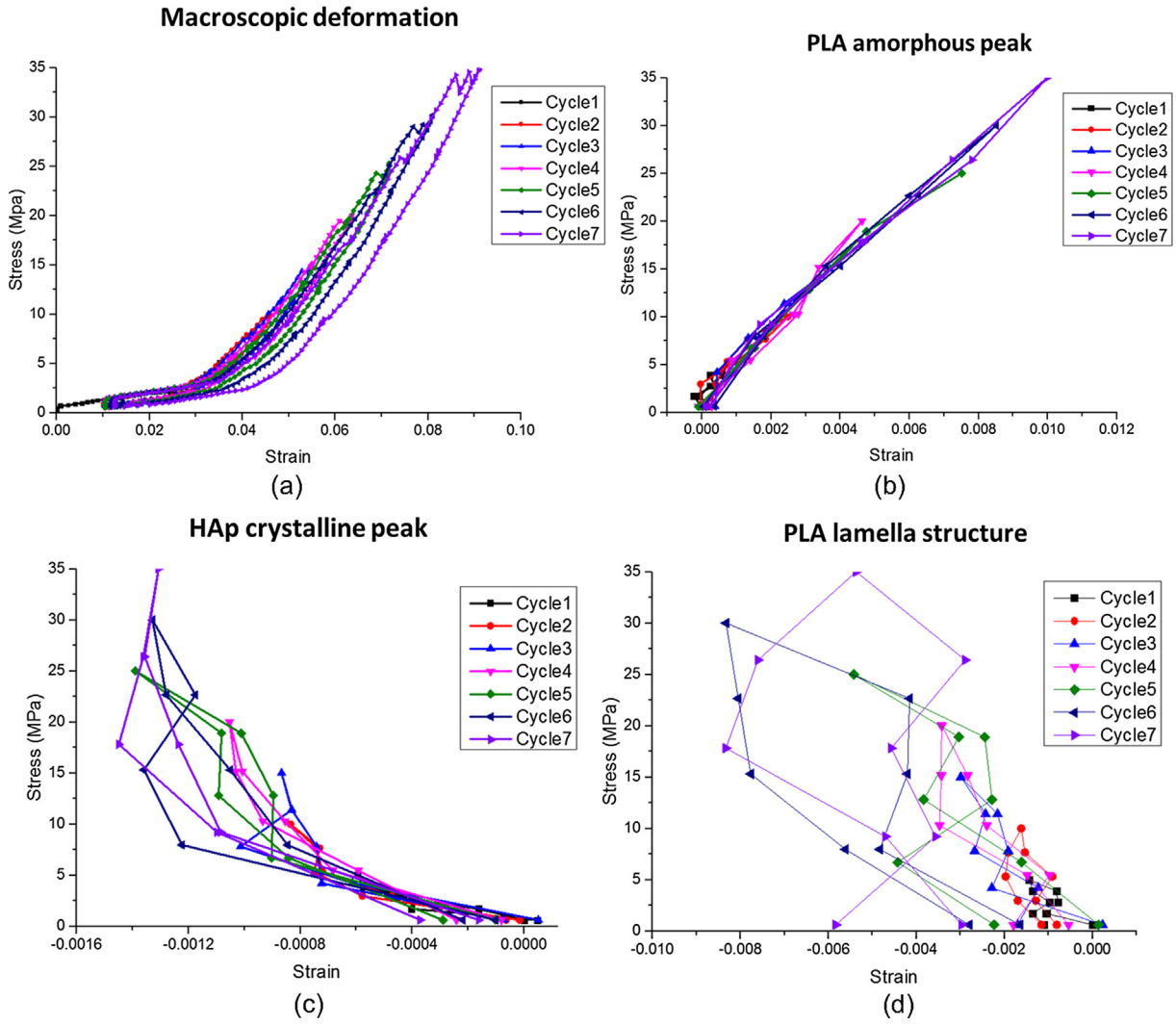

Fig. 2. Mullins effect characterisation of PLA-HAp composite. (a) Macroscopic strain evolution obtained by Deben loading rig at different loading cycles; (b) Strain evolution derived from WAXS patterns of the PLA amorphous peaks at different loading cycles; (d) Strain evolution interpreted from WAXS patterns of the HAp crystallite peaks at different loading cycles; (d) Strain evolution calculated from SAXS patterns of the PLA lamella structure at different loading cycles.

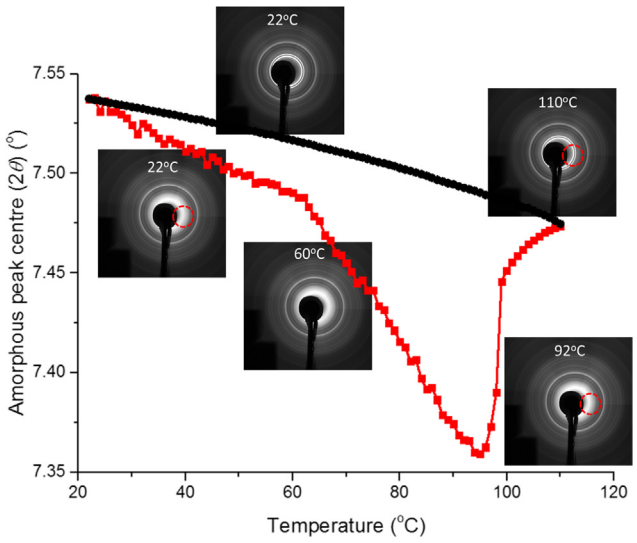

Fig. 3. Thermal properties characterisation of PLA-HAp composite. The PLA composite is heated up from 22 °C to 110 °C (in red) and cooled down to 22 °C (in black) at a constant rate of 2 °C/min. The evolution of the PLA amorphous peak centre position is plotted with temperature. The first phase transition temperature range is identified at around 60 °C and cold crystallisation happens at about 90–100 °C and remains during cooling. This is further confirmed by the inset 2D WAXS patterns at selected temperatures. Red dashed circles show the phase transformation from amorphous peaks (22–92 °C) to crystalline peaks (after 110 °C).

crystallisation above 92 °C. The additional diffraction ring persists during the cooling process down to room temperature, which ends up with a different pattern compared with the original pattern at room temperature before heating. Such comparison reveals the stability of the crystallite phase during cooling, i.e. that irreversible temperature-induced crystallization of the PLA matrix took place.

Thermo-mechanical behaviour

The evolution of the macroscopic strain at the selected temperatures is presented in Fig. 4a. The loading-unloading curves show similar non-linear deformation behaviour as those shown in Fig. 2b. Shift of the curves with temperature can be attributed to the residual strain after each unloading, and softening is observed by comparing the slopes of the unloading curves as the temperature increases. Fig. 4b presents the stress-strain curves for the PLA amorphous peak. It is found that the strain at elevated temperatures is much larger than that at room temperature. Different from the cyclic deformation at room temperature, the strain softening becomes significant when the temperature increases beyond 50 °C. Fig. 4c displays stress-strain curves for HAp filler. Similar to Fig. 2c at room temperature, the HAp filler undergoes non-linear compression even at elevated temperatures, but the magnitude of maximum compressive strain remains small. In contrast, the deformation of PLA amorphous matrix and the overall composite (macroscopically) becomes larger. PLA lamella structure still exhibits non-linear mechanical behaviour and compressive strain, as shown in Fig. 4d. However, it is found to change into tensile state while the temperature increases beyond 52 °C, which indicates the movability enhancement and the progression towards more amorphous formation of the lamella structure.

Shape memory effect

Fig. 5a demonstrates the full shape memory cycle of the PLA amorphous peak over the four stages. At the initial stage under nearly stress-free condition, the strain in the PLA amorphous matrix increases to 0.016 when the sample is heated up from 22 °C to 70 °C, followed by a further increase up to 0.04 in stage I when a load is applied from 0.25 MPa to 3.75 MPa at 70 °C. At stage II, the strain drops from 0.04 to 0.031 while the temperature decreases from 70 °C to 22 °C with the load kept unchanged at 3.75 MPa. A sharp decrease of the strain can be seen from 70 °C to 60 °C. Later at stage III, the strain continues to drop from 0.031 to 0.026 when the sample is unloaded from 3.75 MPa to 0.25 MPa at 22 °C. In the final stage IV (the second stress-free condition), the strain decreases from 0.026 to almost the original level before stage I while the temperature increases again from 22 °C to 70 °C. Compared with stage II, a similar sharp decrease of strain is observed when the temperature increases from 60 °C to 70 °C. In addition, a strong diffraction from crystal structure appears along the meridional direction at stage II, where the sample experiences the 3.75 MPa load at 60 °C. The strong diffraction pattern shown in Fig. 5b persists over stage II, III and IV until finally the temperature reaches 70 °C at stress-free condition. The shape memory effect characteristics were determined by calculating two important quantities [22]: the fixing ratio $\varepsilon_u(n)/\varepsilon_m(n)$, where $\varepsilon_u(n)$ is strain upon unloading and $\varepsilon_m(n)$ is the maximum strain in the n-th cycle; and the recovery ratio $(\varepsilon_u(n) - \varepsilon_p(n))/(\varepsilon_u(n) - \varepsilon_p(n-1))$, where $\varepsilon_p(n)$ is the permanent (residual) strain after heat induced shape recovery.. In our study, the fixing ratio of PLA-HAp composite was calculated to be 65%, and the recovery ratio is almost 100%. At the macroscopic level, the shape memory recovery ratio of the present material was 98% [20], while that of pure PLA amorphous materials has been reported to be 99%, which indicates a minor effect of the HAp filler.

Discussion

The mechanical properties of PLA and its composite are strongly temperature-dependent. Previous research focused on the study of deformation behaviour of PLA material at different temperature ranges, below the glass transition temperature (T_g) [24,25], just above T_g (70–90 °C) [14,26] and at temperatures above cold crystallization (100–150 °C) [15]. The mechanical characterisation in the present study of PLA-based composite focused on the normal service temperature (body temperature) and elevated temperatures below T_g, as well as at the low stress and strain amplitudes, in correspondence with the practical biomedical requirement that PLA needs to maintain its mechanical integrity when exposed to a large number of load cycles with low stress and strain amplitudes [27]. The thermal characteristics of PLA-HAp composite, in particular the PLA amorphous matrix (Fig. 3), were found to be similar to that of pure PLA and PLA-HAp composite reported in the DSC analysis [20], where the endothermic transition was observed at similar range of 50–60 °C and cold crystallization was observed at 90–110 °C.

Regarding the deformation behaviour, for each cycle, the initial increase of the slope of stress-strain curve with increasing load at a given temperature can be attributed to the stress-induced crystallization, as manifested by the diffraction spots appearing in the WAXS patterns (e.g. Figs. 1 and 5). The strain softening of the material during cyclic loading test at room temperature (Fig. 2) and elevated temperature (Fig. 4) are likely to be a competition between the stress-induced crystallization and the increased fraction of the soft amorphous phase. This phenomenon becomes more pronounced at high temperature. The deformation of PLA-HAp composite can be considered as the resistance to stretching of the mechanical network composed of the soft phase (PLA amorphous matrix), the medium phase (PLA lamella structure), and the hard phase (HAp filler). Upon stretching at low temperature, polymer

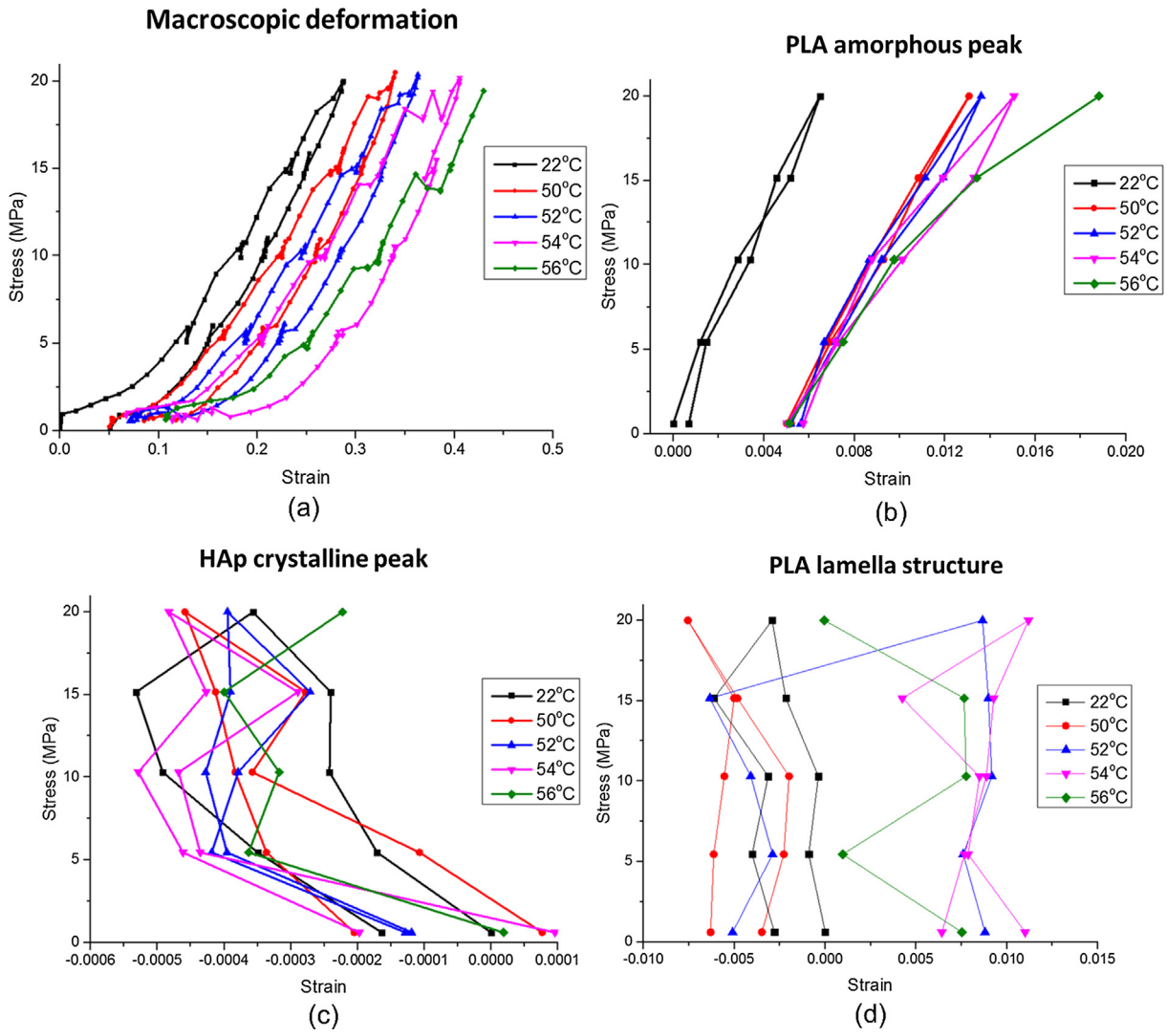

Fig. 4. Thermo-mechanical behaviour of PLA-HAp composite. (a) Macroscopic strain evolution at elevated temperatures (22 °C, 50 °C, 52 °C, 54 °C and 56 °C); (b) Strain evolution derived from WAXS patterns of the PLA amorphous peaks at elevated temperatures; (c) Strain evolution interpreted from WAXS patterns of the HAp crystallite peaks at elevated temperatures. (d) Strain evolution calculated from SAXS patterns of the PLA lamella structure at elevated temperature.

phases are in the glassy state and resist deformation under tensile stress, leading to the high slope of stress-strain curves. With increasing temperature, although the hard phase is little affected owing to its high thermal stability, the soft and the medium phases show significantly enhanced mobility. The resistance to stretching thus decreases, resulting in a rapidly reduced slope of the stress-strain curves, i.e. strain softening. More pronounced strain softening that happens above 50 °C is attributed to the further activation of the amorphous phase induced by the transition from glassy state to highly elastic state [24,25,27].

For each individual phase, the compressive response of HAp filler and PLA lamella structure observed at different temperatures is associated with the structural changes due to the presence of the additional HAp filler. Compression does not occur in the medium and soft segments in elastomer polymers as shown in our previous studies [18,19]. HAp fillers are clearly the stiffest and strongest phase at body temperature compared with PLA amorphous matrix and PLA lamella structure, with evidence from the absolute magnitude of strain under the same tensile load (Fig. 2), i.e. ε (HAp filler) $\ll \varepsilon$ (PLA lamella structure) $< \varepsilon$ (PLA amorphous matrix). HAp filler particles are surrounded by the PLA lamella structure knotted by soft viscous PLA amorphous matrix in the network. The PLA amorphous matrix serves as a "thread knot" when tension is applied to the bulk material, tightening and closing around the PLA lamella structure and HAp filler particles. As a result, a compressive force is generated in the network between the HAp filler particles and PLA lamella structure. Such compression effect persists for HAp filler even when the temperature increases towards the transition value (Fig. 4c), due to the strong thermal stability of HAp filler. On the contrary, the amorphous phase is activated significantly due to the substantial devitrification [24], thus the mobility of PLA lamella structure is enhanced. In addition, the crystallisation process forms more PLA lamella structure and therefore reduces the dimensional spacing, i.e. the PLA lamella long period, and leads to the compression [15]. The newly formed PLA lamella structure further gives additional compression to the HAp filler. The gradually accumulated non-zero residual strain of HAp filler (Fig. 4c) and PLA lamella structure (Fig. 4d) after unloading at each elevated temperature clearly manifests the viscoplastic deformation behaviour of the material.

In order to reveal the internal distribution of HAp particles within PLA matrix in the 3DP sample, cross-sectional synchrotron X-ray tomography images were collected, as shown in Fig. 6(a). These reveal that the dispersion of individual particles of HAp of

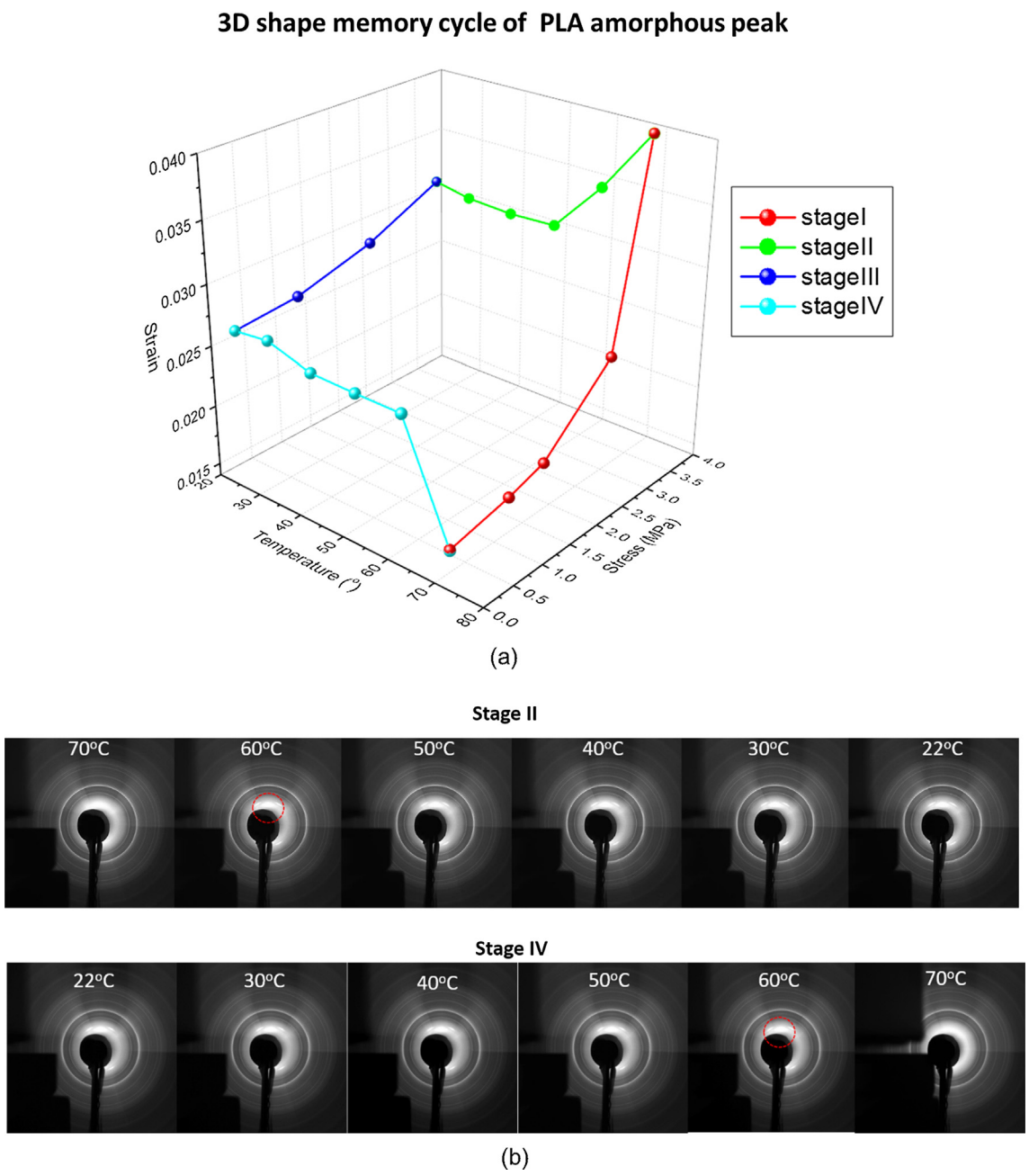

Fig. 5. Shape memory effect characterisation of PLA-HAp composite. (a) 3D shape memory cycle contains four stages (I, II, III and IV), representing loading, cooling, unloading and heating; (b) 2D WAXS patterns for stage II cooling from 70 °C to 22 °C and stage IV heating from 22 °C to 70 °C, showing the appearance of strong diffraction from crystal structure (highlighted in red dashed circle).

micron dimensions was achieved within the material, with some presence of larger particles due to agglomeration, as well as some particle-free regions and pores that are characteristic of 3DP process. Nevertheless, the resulting material showed good mechanical performance that was clearly dominated by the composite response. This arose from the interaction between HAp filler particles, PLA lamella structure and PLA amorphous matrix under loading. The nature of this interaction is schematically illustrated in Fig. 6(b).

In addition, adding bioactive filler to PLA also enhances the shape memory properties and has little influence on the recovery temperature. Although similar characterisation has been reported for other types of polymer acetates [22,28], the 3D thermo-mechanical shape memory plots of the PLA-HAp composite are reported for the first time in Fig. 5 that reveals the details of the coupled thermo-mechanical behaviour. Challenges, however, still remain towards the development of PLA-HAp composites which maintain the biological and mechanical performance but with low actuation temperature close to the body temperature. Further work also needs to be devoted to using the described methodology for *in situ* studies of interaction between such biocompatible materials and cells and/or tissues.

Conclusions

In summary, in this work, PLA-HAp composites manufactured by FFF technique were studied to explore the Mullins effect, thermal properties, thermo-mechanical behaviour, and shape memory effect of this material using *in situ* synchrotron X-ray techniques.

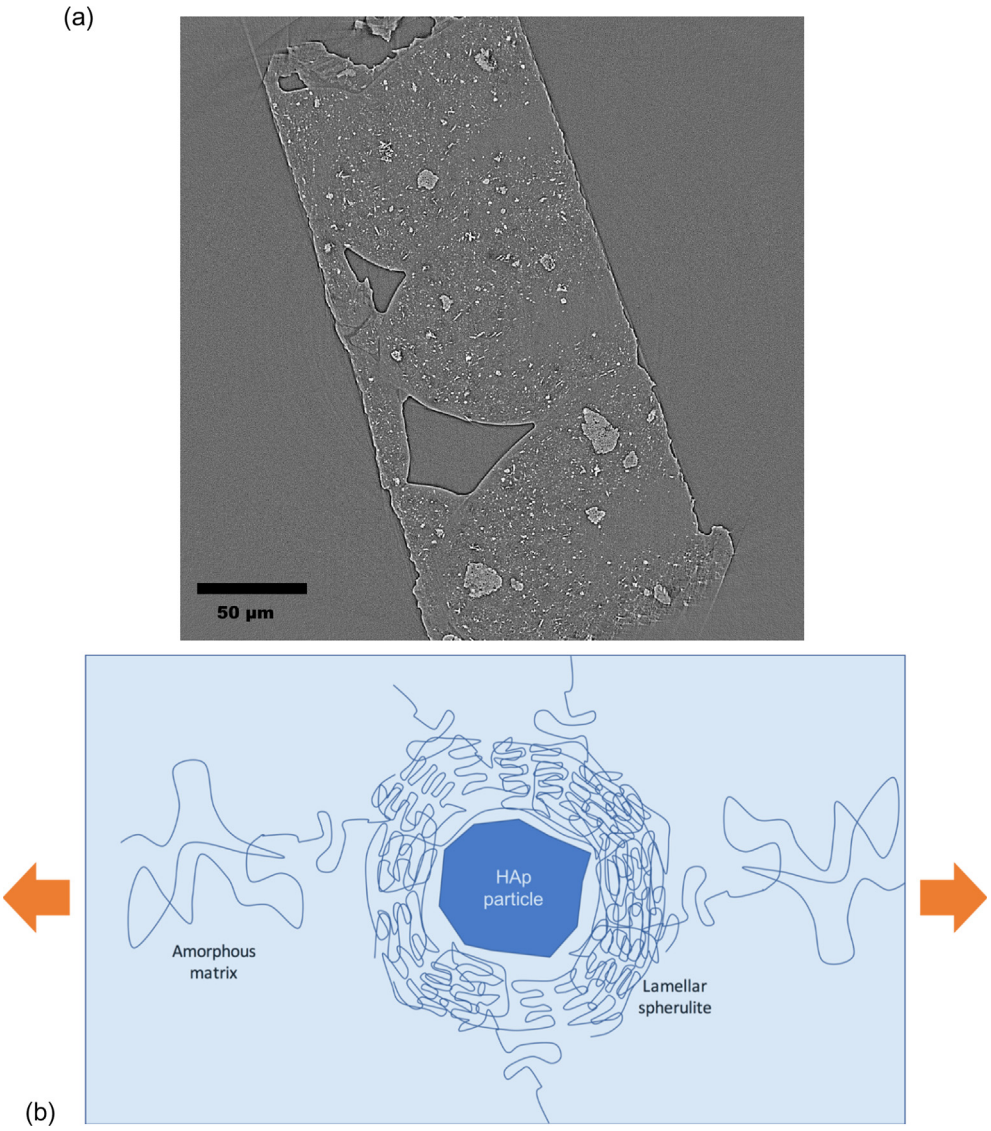

Fig. 6. Illustration of structure and deformation mechanism of PLA-HAp composite. (a) X-ray tomography image of the cross-section of the PLA-HAp composite produced by FDM 3D-printing. (b) Schematic diagram of the system consisting of HAp filler particle(s), PLA lamella structure and PLA amorphous matrix.

The following conclusions were drawn from the series of experiments.

(i) Mullins effect (0–35 MPa, room temperature, cyclic loading): a visible strain softening observed at room temperature is mostly attributed to the non-linear deformation behaviour of the PLA lamella structure and HAp fillers. Compressive strain arises in the soft PLA lamella structure, nearly 5 times of that in strong HAp fillers. Both strains may add additional tension to the PLA amorphous matrix, which would potentially lead to mismatch or potential failure between the matrix and fillers. Reversible crystallisation process is observed where large crystals form or disappear solely dependent on the magnitude of the applied stress.

(ii) Thermal properties (0–110 °C): phase transformation of the PLA amorphous matrix aligns to the thermal characteristics of the PLA-HAp composite measured by DSC. Two phase transformation stages occur in the considered temperature range, with the first one being reversible around 60 °C, while the second one above 92 °C results in irreversible cold crystallisation from amorphous phase.

(iii) Thermo-mechanical behaviour (0–20 MPa, 22–56 °C): the strain softening of the PLA-HAp composite and the PLA amorphous matrix becomes increasingly significant with temperatures, especially above 50 °C. The HAp fillers always exhibit compressive deformation with non-linear mechanical behaviour regardless of temperature. However, the initial compressive state of the PLA lamella can change into tensile state as the temperature exceeds 52 °C.

(iv) Shape memory effect (0–3.75 MPa, 0–70 °C): the process is monitored the first time by synchrotron X-ray techniques and the strain recovery is determined to be nearly 100%, consistent with the macroscopic observation of 98% for the entire composite. This indicates that the addition of 15% wt HAp fillers does not significantly affect the thermal properties of the material but enhances shape memory properties as well as mechanical properties. In addition, the observed chain re-alignment at 60 °C to form crystal structure during the history of shape memory test is attributed to the combined temperature and mechanical load as the mobility at higher temperature increases.

These findings provide characteristics of the PLA-HAp composite and demonstrate the potentials for self-fitting implants for bone replacement, and also open the avenues towards design and functionalities improvement for other biomedical engineering applications. Future work will be devoted to developing 3D printed biocomposites that maintain their mechanical characteristics and biological properties but with close-to-body temperature actuation temperature. This can be potentially achieved by the combination with other biopolymer such as Polycaprolactone (PCL) to make PLA/PCL blends with HAp reinforcement.

Conflict of interest

The authors have declared no conflict of interest.

Compliance with Ethics Requirements

This article does not contain any studies with human or animal subjects.

Acknowledgements

The project was supported by EPSRC RCUK (EP/I020691/1), and project (EP/P005381/1) is acknowledged. Support from Russian Science Foundation (RScF) under project 18-13-00145 is acknowledged. Authors are grateful to Diamond Light Source for the provision of access to beamline B16 under allocations MT17541 and MT21312.

References

[1] Li XM, Cui RR, Sun LW, Aifantis KE, Fan YB, Feng QL, et al. 3D-printed biopolymers for tissue engineering application. Int J Polym Sci 2014.
[2] Tyler B, Gullotti D, Mangraviti A, Utsuki T, Brem H. Polylactic acid (PLA) controlled delivery carriers for biomedical applications. Adv Drug Deliver Rev 2016;15(107):163–75.
[3] Erne P, Schier M, Resink TJ. The road to bioabsorbable stents: reaching clinical reality? Cardiovasc Inter Rad 2006;29(1):11–6.
[4] Wiebe J, Nef HM, Hamm CW. Current status of bioresorbable scaffolds in the treatment of coronary artery disease. J Am Coll Cardiol 2014;64(23):2541–51.
[5] Garg S, Serruys PW. Coronary stents looking forward. J Am Coll Cardiol 2010;56(10):S43–78.
[6] Tamai H, Igaki K, Kyo E, Kosuga K, Kawashima A, Matsui S, et al. Initial and 6-month results of biodegradable poly-l-lactic acid coronary stents in humans. Circulation 2000;102(4):399–404.
[7] Hayman D, Bergerson C, Miller S, Moreno M, Moore JE. The effect of static and dynamic loading on degradation of PLLA stent fibers. J Biomech Eng-Trans ASME 2014;136(8).
[8] van Dijk M, Tunc DC, Smit TH, Higham P, Burger EH, Wuisman PI. *In vitro* and *in vivo* degradation of bioabsorbable PLLA spinal fusion cages. J Biomed Mater Res 2002;63(6):752–9.
[9] Bai HW, Huang CM, Xiu H, Zhang Q, Fu Q. Enhancing mechanical performance of polylactide by tailoring crystal morphology and lamellae orientation with the aid of nucleating agent. Polymer 2014;55(26):6924–34.
[10] Nerkar M, Ramsay JA, Ramsay BA, Kontopoulou M. Dramatic improvements in strain hardening and crystallization kinetics of PLA by simple reactive modification in the melt state. Macromol Mater Eng 2014;299(12):1419–24.
[11] Dorozhkin SV. Bioceramics of calcium orthophosphates. Biomaterials 2010;31(7):1465–85.
[12] Zhang HF, Mao XY, Du ZJ, Jiang WB, Han XG, Zhao DY, et al. Three dimensional printed macroporous polylactic acid/hydroxyapatite composite scaffolds for promoting bone formation in a critical-size rat calvarial defect model. Sci Technol Adv Mater 2016;17(1):136–48.
[13] Barbieri D, Renard AJS, de Bruijn JD, Yuan H. Heterotopic bone formation by nano-apatite containing poly(D,L-lactide) composites. Eur Cells Mater 2010;19:252–61.
[14] Zhou CB, Li HF, Zhang WY, Li JQ, Huang SY, Meng YF, et al. Direct investigations on strain-induced cold crystallization behavior and structure evolutions in amorphous poly(lactic acid) with SAXS and WAXS measurements. Polymer 2016;4(90):111–21.
[15] Zhou CB, Li HF, Zhang WY, Li JQ, Huang SY, Meng YF, et al. Thermal strain-induced cold crystallization of amorphous poly(lactic acid). CrystEngComm 2016;18(18):3237–46.
[16] Kojio K, Matsuo K, Motokucho S, Yoshinaga K, Shimodaira Y, Kimura K. Simultaneous small-angle X-ray scattering/wide-angle X-ray diffraction study of the microdomain structure of polyurethane elastomers during mechanical deformation. Polym J 2011;43(8):692–9.
[17] Zhang H, Scholz AK, Merckel Y, Brieu M, Berghezan D, Kramer EJ, et al. Strain induced nanocavitation and crystallization in natural rubber probed by real time small and wide angle X-ray scattering. J Polym Sci Pol Phys 2013;51(15):1125–38.
[18] Sui T, Baimpas N, Dolbnya IP, Prisacariu C, Korsunsky AM. Multiple-length-scale deformation analysis in a thermoplastic polyurethane. Nat Commun 2015;6(March).
[19] Sui T, Salvati E, Ying S, Sun G, Dolbnya IP, Dragnevski K, et al. Strain softening of nano-scale fuzzy interfaces causes Mullins effect in thermoplastic polyurethane. Sci Rep 2017;7(1):916.
[20] Senatov FS, Niaza KV, Zadorozhnyy MY, Maksimkin AV, Kaloshkin SD, Estrin YZ. Mechanical properties and shape memory effect of 3D-printed PLA-based porous scaffolds. J Mech Behav Biomed 2016;57(April):139–48.
[21] Boote C, Dennis S, Newton RH, Puri H, Meek KM. Collagen fibrils appear more closely packed in the prepupillary cornea: optical and biomechanical implications. Invest Ophth Vis Sci 2003;44(7):2941–8.
[22] Babaahmadi M, Sabzi M, Mandavinia GR, Keramati M. Preparation of amorphous nanocomposites with quick heat triggered shape memory behavior. Polymer 2017;10(112):26–34.
[23] Goderis B, Reynaers H, Scherrenberg R, Mathot VBF, Koch MHJ. Temperature reversible transitions in linear polyethylene studied by TMDSC and time-resolved, temperature-modulated WAXD/SAXS. Macromolecules 2001;34(6):1779–87.
[24] Zhou CB, Guo HL, Li JQ, Huang SY, Li HF, Meng YF, et al. Temperature dependence of poly(lactic acid) mechanical properties. RSC Adv 2016;6(114):113762–72.
[25] Necmi D, Aleksey DD, Naseem T. Effects of temperature on the relaxation behavior of poly(lactic acid). Plast Res 2016.
[26] Stoclet G, Seguela R, Lefebvre JM, Elkoun S, Vanmansart C. Strain-induced molecular ordering in polylactide upon uniaxial stretching. Macromolecules 2010;43(3):1488–98.
[27] Bergstrom JS, Hayman D. An overview of mechanical properties and material modeling of polylactide (PLA) for medical applications. Ann Biomed Eng 2016;44(2):330–40.
[28] Liu C, Qin H, Mather PT. Review of progress in shape-memory polymers. J Mater Chem 2007;17(16):1543–58.